HHS Public Access

Author manuscript

*Acta Biomater*. Author manuscript; available in PMC 2022 November 09.

Published in final edited form as:

*Acta Biomater*. 2019 October 01; 97: 501–512. doi:10.1016/j.actbio.2019.08.002.

# Systematic comparison of methods for determining the *in vivo* biodistribution of porous nanostructured injectable inorganic particles

**Sara Nizzero**[a,b,*], **Feng Li**[a], **Guodong Zhang**[a], **Alessandro Venuta**[a,1], **Carlotta Borsoi**[a], **Junhua Mai**[a], **Haifa Shen**[a,c], **Joy Wolfram**[a,2], **Zheng Li**[a], **Elvin Blanco**[a], **Mauro Ferrari**[a,*,3]

[a]Department of Nanomedicine, Houston Methodist Research Institute, Houston, TX 77030, USA

[b]Applied Physics Graduate Program, Rice University, Houston, TX 77005, USA

[c]Department of Cell and Developmental Biology, Weill Cornell Medicine, New York, NY 10065, USA

## Abstract

With a wide variety of biodistribution measurement techniques reported in the literature, it is important to perform side-by-side comparisons of results obtained with different methods on the same particle platform, to determine differences across methods, highlight advantages and disadvantages, and inform methods selection according to specific applications. Inorganic nanostructured particles (INPs) have gained a central role in the development of injectable delivery vectors thanks to their controllable design, biocompatibility, and favorable degradation kinetic. Thus, accurate determination of *in vivo* biodistribution of INPs is a key aspect of developing and optimizing this class of delivery vectors. In this study, a systematic comparison of spectroscopy (inductively coupled plasma optical emission spectroscopy), fluorescence (*in vivo* imaging system, confocal microscopy, and plate reader), and radiolabeling (gamma counter)-based techniques is performed to assess the accuracy and sensitivity of biodistribution measurements in mice. Each method is evaluated on porous silicon particles, an established and versatile injectable delivery platform. Biodistribution is evaluated in all major organs and compared in terms of absolute results (%ID/g and %ID/organ when possible) and sensitivity (σ%). Finally, we discuss how these results can be extended to inform method selection for other platforms and specific applications, with an

*Corresponding authors. Present address: Mathematics in Medicine program, Houston Methodist Research Institute, Houston, TX 77030, USA. (S. Nizzero)., snizzero@houstonmethodist.org (S. Nizzero), mferrari@ arrowheadpharma.com (M. Ferrari).

[1]Present address: Telethon Institute of Genetics and Medicine, Pozzuoli, Naples 80078, Italy.

[2]Present address: Department of Transplantation/Department of Physiology and Biomedical Engineering, Mayo Clinic, Jacksonville, FL 32224, USA.

[3]Present address: University of St. Thomas, Houston, TX 77006, USA.

Author contributions

S.N. and M.F. designed the research; S.N. performed most experiments, developed the software used for post-processing, and analyzed all data; F.L., G.Z., performed silicon particle radiolabeling; S. N., J.M., and A.V. performed radioactive biodistribution experiments, C.B, H.S., Z.L., E.B., J.W., S.N., and M.F. discussed the results and gave critical comments on the manuscript; S.N. wrote the manuscript.

Disclosure

M.F. serves on the Board of Directors of Arrowhead Pharmaceuticals.

Appendix A. Supplementary data

Supplementary data to this article can be found online at https://doi.org/10.1016/j.actbio.2019.08.002.

outlook to potential benefit for pre-clinical and clinical studies. Overall, this study presents a new practical guide for selection of *in vivo* biodistribution methods that yield quantitative results.

**Keywords**

Biodistribution; ICP-OES; Imaging; Injectable particles; Fluorescence labeling; Radiolabeling

## 1. Introduction

The advancement of both bottom-up and top-down inorganic particle fabrication protocols has paved the way for a new class of porous nano- and micro- structured injectable delivery systems, whose design can be carefully controlled and tailored to specific applications [1]. Among these, porous silicon delivery vectors have demonstrated unique potential in achieving specific physical properties, sustained drug release *in vivo*, and high biocompatibility [2–4]. Moreover, their controllable morphology and composition are associated with favorable degradation kinetics *in vivo*, with a unique potential for prediction of material performances *in vivo* [5]. With the development of new injectable inorganic particles for *in vivo* applications, the evaluation of biodistribution has acquired a new role in determining the potential for effective translation. For example, the systematic analysis of nanoparticle delivery to tumors has highlighted the necessity to improve delivery specificity of injectable drug carriers in order to improve therapeutic outcome [6]. Moreover, the development of quantitative *in vivo* biodistribution protocols for inorganic particles has brought about a new understanding of *in vivo* clearance mechanisms of hard nanomaterial clearance [7]. Recently, the systematic evaluation of *in vivo* biodistribution of injectable mesoporous silicon particles has highlighted the quantitative role of design parameters such as size and charge, as well as administration route on pharmacokinetic and organ accumulation [8]. These and other works have highlighted the importance of identifying quantitative biodistribution methods for injectable inorganic delivery vectors in order to optimize their design. While others have previously reviewed and collected several different results on biodistribution from literature and compiled comprehensive reviews on advantages and disadvantages of biodistribution methods for the detection of nanoparticles biodistribution [9], it is important to perform systematic evaluation of performances of different biodistribution methods on the same platform, to allow for side-by-side comparison.

Determining *in vivo* biodistribution is a critical step to evaluate the performance of inorganic particles for several biomedical applications [10]. Several different methods are currently employed to evaluate particle biodistribution in preclinical studies. All of these methods have different characteristics that make them advantageous for specific applications. Recently, Arms et al. have collected and reviewed different nanoparticle biodistribution protocols [9], and compared them highlighting different aspects such as: quantitative vs qualitative measurements, sample type (whole animal, whole organ/tissue, tissue section), and study duration. While this review provides a solid ground to select techniques according to the application needed, it remains essential to know how different techniques perform on evaluating biodistribution of the same platform, and whether or

not bias is introduced switching across techniques. In this work we select five techniques which are commonly employed in the evaluation of biodistribution for inorganic particles in preclinical studies: inductively coupled plasma - optical emission spectroscopy (ICP-OES), *in vivo* imaging system (IVIS), confocal microscopy of tissue sections, fluorescence measurement of homogenized organs, and radiolabeling. The first method investigated is ICP-OES, a direct method that can be employed for inorganic materials such as Si. As a direct method, it does not require labeling when employed on inorganic particles. ICP-OES has been widely utilized to optimize porous silicon microparticle design to achieve tailored biodistribution [11–13]. The same technique was utilized in the work by S. Chinde et al. [14] to investigate the biodistribution of nano and micron-sized tungsten oxide in rats, and in the paper by Al Zaki et al. [15] to localize gold-loaded polymeric micelles in nude mice. The same technique was also employed by Tanaka et al. [16] to assess the biodistribution of siRNA-loaded mesoporous silicon particles in an ovarian cancer murine model. ICP-MS was employed by Ganesh et al. [17], who determined the biodistribution of i.v. injected cisplatin loaded in CD44 targeted hyaluronic acid (HA) nanoparticles (NPs) in mice bearing cisplatin resistant $A549^{DDP}$ tumors.

The next three methods are based on fluorescence, so they require either intrinsic nanoparticle fluorescence or fluorescent labeling. These methods are often used in complement with each other, especially when platforms tested are intrinsically fluorescent. *In vivo* optical imaging (IVIS) is a technique used to detect fluorescent particles or drugs based on their emission upon laser excitation. Typically, dyes for this purpose are selected in the near infrared range (600–1000 nm) to minimize attenuation by biological tissue absorption [18–20]. For example, Lee et al. have measured biodistribution of Iron-Oxide nanoparticles as measured with ex vivo IVIS imaging [21]. In the paper by Cong et al. [22], IVIS is used for comparison with multispectral optoacustic tomography (MSOT) in order to determine the intratumoral distribution of polymeric micelles. IVIS was also used in the paper by Gusliakova et al. [23] to investigate the biodistribution of vaterite particles. In another work by Kumar et al. [24], IVIS is utilized to determine the biodistribution of micelles encapsulating Cy5.5-let-7b and GDC-0449 following intravenous injection in orthotopic pancreatic tumor-bearing NSG mice. IVIS has also been utilized by Hollis et al. [25] to localize paclitaxel hybrid nanocrystals that were previously intravenously administered to a HT-29 colon cancer xenograft murine model. Another work by M. Deshmukh (5) used IVIS to investigate the biodistribution of intravenous dye-labeled stabilized aggregated nanogel particles (DYE-SANPs) in rats.

While confocal imaging is generally considered a qualitative measurement, it is frequently used as a quantitative measure to evaluate accumulation of particles or drugs in different tissue compartments such as certain immune cells, blood vessels, tumor areas. For example, Vasconcelos et al. used a combination of histological analysis and fluorescence imaging to quantify $ZrO_2$ particle debris accumulation in prostate tissues [26]. Similarly, Van de Ven et al. used confocal imaging to quantify particle co-localization with macrophages in several organs [11].

Recently, fluorescent particle biodistribution has been evaluated through measurement of homogenized tissues, a technique that allows to reduce or eliminate organ attenuation via

serial dilutions and calibration. Bernhard et al. used organ homogenization to measure fluorescently labeled Nimotuzumab biodistribution in several organs [27] following a modified method developed by Oliveira et al. [28]. Later on, Wolfram et al. used a similar technique to evaluate particle biodistribution in several organs upon chloroquine pre-treatment [29]. However, in both cases no standard was used for calibration, thus results could not be expressed in terms of %ID. The fifth method requires labeling with a radioactive isotope and, because of its sensitivity, is generally regarded as the golden standard for evaluation of *in vivo* particle biodistribution. Thanks to their high sensitivity and throughout put at low labeling amount, radioactive labeling has been widely used to investigate the effect of variables such as size, shape, and surface modification on inorganic particle biodistribution. For example, Licciardelli et al. have used $^{64}$Cu labeling to investigate the differences and similarities of biodistribution of ultrasmall carbon and silicon nanoparticles, very sensitively highlighting the role of surface charge in biodistribution. This work is aimed at identifying and comparing quantitative methods for measuring biodistribution that can help rationalize the choice and further optimization of biodistribution methods for preclinical work.

Within the class of inorganic injectable delivery vectors, porous silicon particles (PSPs) fabricated via semiconductor microlithography [30] present unique advantages in terms of increased therapeutic efficacy and reduced side effects thanks to their tumoritropic accumulation, or *physical targeting*: a favorable biodistribution achieved upon careful optimization of physical design parameters [11,31]. While particles smaller then 5–8 nm preferentially undergo renal clearance [32], particle of size bigger then 20 nm accumulate in liver, spleen, and lungs, with discoidal particles showing preferential accumulation to lungs [33]. In particular, discoidal design of porous silicon particles has been shown to result in enhanced tumor accumulation [11,34] with particles of ~1 μm diameter showing preferential accumulation to primary breast tumor tissues [13] where particles with diameter larger then 2 μm display increased accumulation to lung vasculature, further enhanced by the presence of tumors. These discoidal particles have been previously demonstrated great potential for *in vivo* applications. Part of their favorable *in vivo* properties are due to their highly porous nature with pore size is below 60 nm [35] and degradation kinetic dependent on size [36]. In particular, the *in vivo* safety of i.v. administration (both intravenous and retro-orbital administration, single and multiple dose) of these particles has been previously proven [3], and their therapeutic potential has been shown for *in vivo* delivery of chemotherapeutic drugs [37]. Thus, we have chosen to perform experiments with these particles which not only have shown great potential for *in vivo* application, but also exhibit a geometrical design that favors organotropic accumulation to lungs, an organ of great interest for many applications but typically difficult to target with nanoparticle delivery. PSPs are fabricated conforming to the United States Food and Drug Administration's (FDA's) current Good Manufacturing Practice (cGMP) regulations. Physical targeting properties have brought about advancements in several applications where PSPs have been employed as delivery vectors for different types of nanoparticles and therapeutic agents [34]. Particles were functionalized with APTES prior to injection to enhance loading and conjugation capacity, and facilitate particle degradation and clearance [12,36]. APTES-based labeling procedures have been previously developed into well-established protocols by

this and other labs, to functionalize silicon particles prior to fluorescent and radioactive labeling, with high stability and reproducibility. For the type of labeling employed in this work, pre-functionalization of PSP with APTES was used to mediate conjugation with Alexa Succinimidyl Ester [13,29,38] and Deferoxamine (DFO) [29,39]. Additional positive implications of APTES functionalization in terms of drug loading, toxicity and *in vivo* degradation have been amply discussed in literature [40]. For example, APTES has been shown to improve particle stability in aqueous media [13,41,42], result in >90% degradation in physiological fluids (Fetal Bovine Serum) within 20 h of incubation, and have no pro-inflammatory effect upon co-incubation with both human macrophages and endothelial cells [12].

Previous studies have shown that these particles maintain integral shape and size for the first several hours [13,43]. PSPs have been successfully exploited for the *in vivo* systemic delivery of siRNA for the knockdown of STAT3, which resulted in a significant reduction of tumor cancer stem cells, at low enough doses to prevent acute immune response or sub-acute toxicity [44]. Combination of physical and biological targeting of overexpressed E-selectin has enabled the application of the STAT3 knockdown strategy to bone marrow metastasis of both MDA-MB-231 and MCF-7 tumors at specific disease stages, significantly extending their survival rates [45]. More recently, PSPs have been used as base platform for the development of injectable nanoparticle generators for the treatment of lung metastasis of triple negative breast cancer, inducing functional cure of 40–50% of MDA-MB-231 and 4T1 models of metastatic breast cancer [37]. Moreover, this platform exhibits potential for the achievement of organotropic biodistribution profiles through the combination of physical targeting with preconditioning strategies [29]. Overall, these and other results have shown that a favorable biodistribution (preferential drug accumulation to the target site) can be achieved with the use of PSPs, which can be key to increasing therapeutic efficacy and reducing side effects [33,46].

This study provides a systematic comparison of commonly used assays to evaluate biodistribution. We will perform this comparison using PSPs as testing platform. We will analyze the result of each method side by side and compare them in terms of absolute results and sensitivity, to support selection of appropriate protocols for the evaluation of *in vivo* biodistribution of injectable inorganic particles for drug delivery. For these biodistribution studies we selected bigger particles (nominal size: 2.6 μm x 0.7 μm) that have previously shown great potential by IV injection [37]. Furthermore, a time point of 15 min was selected, where, for the particle size studies, PSP are mostly cleared from circulation, but degradation and systemic clearance processes have not begun yet. This allows complete decoupling of accumulation kinetic from clearance kinetic. First, all methods are analyzed individually and results are shown in terms of %ID/g or equivalent units. Results from optical methods are also compared with each other. Then, results are shown in terms of %ID/organ, for methods where such calculation is possible. Finally, methods where a calculation of % ID/g and %ID/organ are possible are quantitatively compared both in terms of absolute results and sensitivity (σ%).

## 2. Materials and methods

### 2.1. Particle fabrication

Disk-shaped PSPs (2600 nm x 700 nm) were fabricated using photolithography and electrochemical etching according to a previously reported method [38,47]. PSPs were then functionalized with (3-Aminopropyl)triethoxysilane (APTES) and stored dried at 4 °C.

### 2.2. Animal studies

Animal studies were approved by the Institutional Animal Care and Use Committee (IACUC) at the Houston Methodist Research Institute and performed in adherence to the National Institutes of Health Guide for the Care and Use of Laboratory Animals. Female BALB/c mice were purchased from Charles River Laboratories (Wilmington, MA). For all biodistribution studies, silicon particles ($10 \times 10^7$/mouse) were sonicated to resuspend them in solution and then immediately intravenously (i.v.) injected (tail vein). Terminal cardiac puncture was performed 15 min post-injection for blood collection, using needles pre-rinsed in EDTA (0.5 M; pH 8; Thermofisher Scientific, Waltham, MA). Organs were then collected and weighed, then processed for each method as described below.

### 2.3. Fluorescence labeling of PSPs

APTES-conjugated particles (APSPs) were further conjugated to Alexa Fluor 647 succinimidyl (NHS) Ester (Life Technologies, Carlsbad, CA) as previously described [11,48]. Briefly, $50 \times 10^7$ APSPs were dispersed in 3 mL of a 20% TEA solution in Dimethyl Sulfoxide (DMSO), then 200 μL of Alexa were added and the solution and mixed overnight. Particles were then washed in sterile water five times via centrifugation (1000g; 10 min) and stored dried at 4 °C.

### 2.4. Radioactive labeling of PSPs

For radiolabeling studies, PSPs were labeled with $^{89}$Zr following a recently published procedure [29]. Briefly, APSPs were dispersed in anhydrous dimethylformamide (DMF; $5 \times 10^9$ particles/mL; Sigma-Aldrich, St. Louis, MO) for chelation. Disuccinimidyl substrate (DSS; 2 mg/mL in DMF; 100 μL; Thermo Fisher Scientific, Waltham, MA) and triethylene amine (TEA; 20 μL; Sigma-Aldrich, St. Louis, MO) were added to the solution and mixed for 30 min at room temperature (RT). The solution was washed twice through centrifugation (1500g; 10 min) and mixed with DFO, washed, and vacuum dried. DFO-chelated particles were then added to a $^{89}$Zr solution ($^{89}$Zr-oxalate dispersed in oxalic acid and $Na_2CO_{3aq}$ 1Suc-cinimidyl M, purchased from Washington State University, Pullman, WA), sonicated, mixed for two hours, and then washed through centrifugation. The labeled particles were utilized within 10 h from the start of the labeling procedure.

### 2.5. Biodistribution measurements with ICP-OES

For ICP-OES, a final volume of 120 μL ($60 \times 10^6$/mouse) APSPs was injected in each mouse. After 15 min, mice were sacrificed and major organs collected, weighed, and homogenized with a T25 Digital Ultra Turrax Homogenizer (Ika-Werke, Staufen im Breisgau, Germany; $25 \times 10^3$ rpm; 590 g; 1 min/organ) in a solution of EthOH:NaOH

(0.01 N) 20:80 v/v. Next, samples were sealed with parafilm to prevent evaporation, and digested for 48/72 h, RT. Samples were subsequently spun down (5000 g; 30 min), and clear supernatants were further diluted 0.12 v/v NaOH/EtOH. Schematic of organ processing for ICP is reported in Supplementary Material S5. Silicon content was detected with the Varian 720-ES ICP-OES (Varian Palo Alto, CA) at 250.69, 251.61, and 288.158 nm, using yttrium (1 ppm) as an internal control for normalization. A 10–12 point calibration curve was built for each measurement wavelength using calibration concentrations and measurements from different days. Si concentrations in organs (μg/g) were estimated using measured intensities and averaged across values from the three different Si wavelengths measurements. Silicon content was normalized to the injected dose to obtain the %ID.

### 2.6. Biodistribution via IVIS

For all fluorescence biodistribution studies (intravital measurement, IVIS, confocal, homogenized organs), fluorescent particles were dispersed in sterile water for injection. A final volume of 120 μL ($60 \times 10^6$ particles/mouse) was injected in each mouse. For *in vivo* imaging system (IVIS) studies, liver, spleen, lungs, kidneys, and blood were collected and imaged immediately after euthanasia. Regions of interest from the images obtained were identified and quantified as average radiance using Living Image® software 4.0 (Caliper, Alameda, CA).

### 2.7. Biodistribution via confocal microscopy

For confocal studies, frozen organ sections were stained with 4′,6-Diamidine-2′-phenylindole dihydrochloride (DAPI) and imaged with a Nikon confocal microscope (standard confocal microscope resolution determined by the Abbe diffraction limit as $\delta_{diff} = 0.61\ \lambda NA$ [49]). Several slides from multiple animals were analyzed for spleen and lungs (N = 8), and liver (N = 16). A custom MATLAB software was developed to speed up analysis and semi automatize the process (source code in supplementary material, downloadable as open source). A schematic representation and explanation of the working principle is reported in Supplementary Material S4. Briefly, each single channel image (channel corresponding to particle emission) is converted to a grayscale image and the background (calculated on a user input area) is subtracted. Then, the total intensity/field of view (FOV) is integrated over the whole area for each image. To convert the intensity/FOV to #/FOV, a single particle intensity histogram is built based on user-selected single particles. The intensity of each image is divided by the average of single particle intensity, leading to particle numbers. The histogram of single particle intensities is given as output to provide a visual quality control to the user: for them to be truly single particles, the histogram should qualitatively resemble a Gaussian distribution.

### 2.8. Biodistribution via fluorescence of organ homogenates

For fluorescence measurements of homogenized organs, homogenization of pre-weighed organs in PBS (1 g/3 mL) was carried out with a T25 Digital Ultra Turrax Homogenizer (Ika-Werke, Staufen im Breisgau, Germany; $25 \times 10^3$rpm; 590 g; 1 min/organ). The integrated fluorescence intensity (Ex = 640 nm, slit aperture = 20 nm) of serial dilution of blood and homogenized organ samples was measured in the spectral band defined as 678 ± 20 nm with a Synergy H4 Hybrid Microplate Reader (BioTek, Winooski, VT).

Fluorescence background from blood and organs from untreated mice was subtracted from the measured values to account for autofluorescence. Measured fluorescence was further corrected for attenuation from organ homogenate absorption [50] with the use of a calibration curve. The percentage-injected dose (%ID) was calculated comparing the corrected fluorescence measured in 6.25 μg homogenized tissue in 100 μL PBS with the fluorescence of injected particle. This method was optimized from that described in previous studies [29] and its protocol is reviewed in Supplementary Materials S7. Fluorescence labeling was characterized in Supplementary Material S3.

### 2.9. Biodistribution measurements with radiolabeling

$^{89}$Zr-labeled particles were dispersed in saline and 100 μL-150 μL (60 μCi-100 μCi, $60 \times 10^6$ PSPs/mouse) were injected in each mouse. Organ and blood activity was measured in counts per minutes (cpm) with a 2470 Wizard Automatic Gamma Counter (Perkin Elmer, Waltham, MA), allowing for decay of saturated organs. Measurements were corrected for background and decay with the use of a standard.

### 2.10. Radiolabeling stability

Radiolabeling stability was measured through radio-thin-layer chromatography in mouse plasma diluted 1:1 in PBS. Radiolabeled particles were washed and incubated for 1 h in diluted mouse plasma, then radio-TLC was measured again and compared to purified particle signal.

### 2.11. Methods comparison

All biodistribution detection methods were analyzed using relative measurements of intensity/field of view or %ID/g when possible. Since optical methods such as IVIS and confocal imaging rely on imaging of a tissue section or surface (S), the most proper way to compare results with a volume (V)-based detection method is through comparison of %ID/g with particle intensity or number/ FOV, since V = S.d, d being the depth of analyzed tissue, which for optical methods is a constant proportional to a wavelength dependent number, limited by Abbe's diffraction limit. A detailed mathematical justification for this comparison is reported in Supplementary Material S6. When possible, the %ID per organ is also calculated. Since tissue attenuation makes it not possible to perform an absolute comparison across fluorescent methods, a relative biodistribution comparison (different scales) across the three fluorescence biodistribution methods is performed. When shown, percentage errors are also calculated as an additional metric for comparison as σ/value for each organ.

### 2.12. Statistical analysis

Statistical analysis was performed with GraphPad Prism 6 software (GraphPad Software, Inc., La Jolla, CA, USA). Biodistribution results are presented as mean ± standard deviation (σ), for each group. Percentage errors (σ%) are calculated as r/mean value for each organ.

# 3. Results

## 3.1 Biodistribution via ICP-OES

ICP can be used to evaluate biodistribution of inorganic materials without the need of additional labeling, and potential consequent surface modification.

As shown by scanning electron microscopy (SEM, Fig. 1a), the size and shape of PSPs are well-defined and regular across production. After digestion, Si content is measured in all different organs and results are shown in terms of %ID/g for the organs where Si traces are detectable above the limit of blank of the instrument (Fig. 1b). “Notably, results in Fig. 1b are reported as %ID/g, where the % injected dose recovered in each organ is normalized by each organ weight. Average organ weights are reported in Fig. 1c.”

The liver is the organ with the major uptake potential, where 83% ± 18% ID/g accumulates. Following the liver, lungs and spleen accumulate 48% ± 22% ID/g, and 14% ± 13% ID/g, respectively. Additionally, at the time of sacrifice (15 min post injection), 40% ± 34% ID/g remains in circulation. Results shown are presented after background subtraction.

## 3.2 Biodistribution via IVIS

IVIS imaging is one of the most widely used methods to determine biodistribution, as results can be rapidly obtained in live animals or dissected organs.

For this method, organs are collected and imaged immediately after sacrifice (Fig. 2a). Radiant efficiency is then calculated and plotted as result (Fig. 2b). As estimated with this method, the radiant efficiency measured in each organ was: $23\pm5\cdot10^5$ for liver, $48\pm11\cdot10^5$ for lungs, $2\pm1\cdot10^5$ for spleen, $5\pm1\cdot10^5$ for kidneys. No signal was detected in blood.

## 3.3 Biodistribution via confocal microscopy

Confocal microscopy is complementary to IVIS, especially in terms of determining intra-organ heterogeneity in particle accumulation.

For each organ, several images (N = 8–16, Fig. 3a) were analyzed to count the number of particles per field of view (#/FOV) from the particle channel. Biodistribution results are then presented in terms of #/FOV in each organ (Fig. 3b). With this method, the number of particles/FOV detected in each organ are: 107 ± 28 in the liver, 914 ± 295 in lungs, and 73 ± 31 in the spleen. Other organs are not included, as PSPs were not detected in them.

## 3.4 Biodistribution via fluorescence of organ homogenates

The third optical method used in this study is based on measuring the fluorescence intensity of homogenized organs. A schematic representation of the protocol is reported in Supplementary Fig. S4. Fig. 4 reports biodistribution results obtained with this procedure. Linearity of particle fluorescence as a function of particle concentration (Fig. 4a) and organ absorption as a function of organ concentration (Fig. 4b) was verified. Experimental parameters used (ID, time point, and organ dilution factors) were optimized to be within the linear range of both fluorescence emission and organ attenuation, which enabled the use of linear correction factors. Those correction factors (Fig. 4c) were calculated as the

ratio between the intensity of a known amount of particles in PBS and the intensity of the same amount in organ homogenates, and validity was verified within the whole range of concentrations used (as expected within a linear range of emission and absorption). Intensities were measured using serial dilutions for each organ (Fig. 4d). Calculated biodistribution was similar with all serial dilutions (Fig. 4d), confirming once more the linearity of the system (Supplementary Material S8). Fluorescence emission values were converted to %ID by dividing the corrected intensity per organ with the total injected fluorescence. Results are then presented in terms of %ID/g (Fig. 4e), as calculated from measurements on 6.25 μg tissue in 100 μL PBS. Particles distribute across organs in the amount of: 22% ± 5% ID/g in the liver, 42% ± 6% ID/g in the lungs, 9% ± 3% ID/g in the spleen, while 5% ± 1% ID/g remains in circulation (blood). No significant signal is detected in any other compartment. For reference, biodistribution patterns as estimated through IVIS (Fig. 4f) and confocal imaging (Fig. 4g) are compared to homogenized organ fluorescence (gray bars in Fig. 4f and g). Scales are adjusted to facilitate result comparison.

### 3.5. Biodistribution via radiolabeling

PSP labeling via $^{89}$Zr isotope (Fig. 5a) is used to enable highly sensitive measurements of biodistribution through radioactivity measurement. The labeling stability is verified by comparing results from radio-TLC after purification (Fig. 5b) with results obtained after incubation in mouse plasma (Fig. 5c). Particles are detected in different organs in the amount of: 96% ± 9% ID/g in liver, 51% ±15% ID/g in lungs, 62% ± 10% ID/g in spleen, 3%±1% ID/g in kidneys, 2.1% ± 0.2% ID/g in blood, 1.1% ± 0.3% ID/g in heart, 0.27% ± 0.07 in the gastrointestinal track, 0.62% ± 0.05% in muscle.

### 3.6. Comparison across quantitative methods

We refer to quantitative methods those where it is possible to convert method-specific numerical results into a standardized measurement in terms of %ID and %ID/g.

Fig. 6 reports a summary and comparison of biodistribution obtained with ICP-OES, fluorescence of homogenized organs, and radiolabeling. Results reported as %ID/g for fluorescence (Fig. 6a), ICP-OES (Fig. 6b) and radiolabeling (Fig. 6c) for lungs are similar across all methods. Liver accumulation as measured with radiolabeling and ICP gives comparable values, while liver accumulation estimated via fluorescence is roughly half. Spleen content as measured through radiolabeling is about 2/3 as that of the liver, but it is significantly reduced in ICP and fluorescence methods. Spleen content is similar between ICP and fluorescence.

Among the three methods, the only one where a significant signal is detected in the kidneys is the fluorescent one. However, measurement in kidneys is low with all three techniques, which is due to the size cutoff for kidneys uptake. Blood content is the highest for ICP, followed by fluorescence, and it is minimal for radiolabeling. It should be noted that the error of the ICP blood measurement is on the same order of magnitude of the value itself, thus suggesting that the quantification of circulating PSP should not be obtained from ICP measurement. The value of blood content as estimated through radiolabeling and fluorescent biodistribution methods is below 10%, thus confirming the short circulation time. Errors on

the %ID/g are below 20% for all methods, with minimum errors for fluorescence. When analyzing the %ID/organ (Fig. 6g-h-i), the major accumulation organ is the liver for all three methods, followed by the lungs. For ICP, the amount of PSP in circulation is the highest (25% ID), followed by fluorescence (20% ID), and radiolabeling (<5%1D). Errors across organs (Fig. 6j-k-l) are the highest when measured with ICP (<40%), followed by fluorescence (<10%) and radiolabeling (~<5%).

## 4 Discussion

This study involves a systematic comparison of commonly used biodistribution measurement methods, with the end goal of providing a rational guide for selection of complement techniques for evaluation of *in vivo* biodistribution of injectable inorganic particles. First, a label-free method to evaluate biodistribution for inorganic particles is analyzed: ICP-OES. Results with this measurement were sensitive enough to detect signals in liver, spleen, lungs and blood, although with significant standard deviations (between 10% and 50% of the measurement). This direct detection method offers the advantage of not requiring additional labeling. However, the procedure of organ digestion can be time consuming (4–6 days), and a significant amount of tissues is necessary to obtain results that can be distinguished from the background (limit of blank). For applications where sensitivity is a priority, the use of additional labeling techniques can be very useful, with the advantage of obtaining a more sensitive measurement that requires lower amount of tissue.

Among the methods that require additional labeling, fluorescence-based detection methods are frequently employed to evaluate particle biodistribution in preclinical studies. The most common techniques are: IVIS, confocal imaging, and measuring the fluorescence intensity of homogenized organs. These methods are popular due to the prevalence of fluorescence labeling protocols, as well as the existence of many particles that already exhibit fluorescence for biomedical applications [51,52]. Most fluorescent detection methods are affected by background signals and tissue attenuation and scattering, which dramatically affects the measured fluorescence [53]. These artifacts can be minimized for by selecting a fluorophore with a spectrum outside of the autofluorescence and tissue optical absorption range [19]. In addition, when possible fluorescence background can be removed by subtracting the signal of control tissues, while tissue attenuation can be accounted for with the use of calibration curves.

In particular, while IVIS is a time-efficient method for obtaining results, it generally leads to a systematic and unavoidable underestimation of particle content for densely packed and optically absorbing organs. In fact, light penetration in tissue is limited to surface structures and decays exponentially with increasing tissue thickness [54]. This effect can be attenuated, but not eliminated, with the use of near-infrared dyes, which can achieve up to a few mm of penetration depth. Despite the homogeneity in distribution as seen from IVIS imaging, estimated biodistribution shows high error bars and low sensitivity, which can hinder interesting biodistribution features. Notably, in this method fluorescence is coming from particles emitting through densely packed and optically opaque tissues, which results in a systematically underestimated measurement. More importantly, fluorescence attenuation varies among different organs, and this can produce misleading results if this method is used

to evaluate inter-organ biodistribution. However, this method still presents an extremely time efficient technique to obtain general qualitative results of biodistribution, especially when comparing accumulation in the same organ between animals.

Confocal imaging offers an advantage over whole organ fluorescence biodistribution methods in overcoming tissue absorption since only emission from particles in a narrow focal plane is detected. However, other factors contribute to the qualitative nature of biodistribution results obtained through confocal imaging such as: pH-induced change in fluorescence upon particle internalization in lysosome [55,56] or cytosol [56] compartments, fluorescence alteration due to non-specific protein binding [57]. Gottstein et al. have developed a mathematical calibration approach that integrates flow cytometry and confocal imaging to quantitatively assess particle internalization, proving the necessity of a calibration factor to make these methods quantitative. While this protocol is very valuable when precise quantification of internalized particles is needed, it requires the combination of several assays with mathematical analysis and calibration, which may be impractical for many *in vivo* applications. Thus, it is still important to understand the value of biodisitribution evaluation with traditional confocal imaging in comparison with other techniques. In fact, often times a quantitative technique is used to measure organ accumulation in terms of %ID while confocal microscopy is used instead to quantify differences in organ compartmentalization.

Although confocal microscopy is not limited by organ attenuation, the capability of reconstructing biodistribution patterns in the entire organ is impractical due the requirement of a large amount of tissue sections. Nevertheless, confocal images can provide microscopic information that sheds light on intra-organ heterogeneity in particle accumulation, as well as potentially providing a mechanistic understanding of organotropism. This method can be especially useful to visualize particles in conjunction with immunofluorescently labeled tissue components. Although the combined use of confocal imaging and IVIS provides information about both macroscopic (global) and microscopic (local) aspects of biodistribution, they are in many cases unable to give quantitative unbiased measurements. Both background and attenuation can correction can be achieved with the measurement of fluorescence of organ homogenates and the use of a calibration curve. Fluorescence measurements of whole organ homogenates overcome the drawbacks of IVIS and confocal imaging, as organ attenuation can be eliminated with the use of calibration factors and whole organ fluorescence can be measured by sampling a homogenously homogenized organ. Notably, the correction factor for lungs in our results is the closest to 1, which corresponds to low organ attenuation (clear tissue). On the other hand, liver and blood require the highest correction, as expected for dark and highly absorbing tissues. These results are in agreement with results from the work of Bernhard et al. where biodistribution from homogenized organs was compared with biodistribution via *in vivo* imaging [27]. While the overall behavior of data was qualitative comparable between both techniques, some significant differences emerged especially when comparing different time points and different organs. For example, when measuring accumulation through organ homogenization, the highest accumulation after blood was detected in liver and tumors, with a significant increase in xenograph accumulation between 24 h and 72 h, which did not appear from ex vivo IVIS imaging. Moreover, overall measurements from homogenized organs resulted more

sensitive compared to ex vivo IVIS, confirming our results on sensitivity. Likewise, in the work by Diagaradjane et al. both IVIS and fluorescence of tissue homogenate were analyzed in order to assess the biodistribution of near-infrared quantum dots in mice bearing HCT116 xenograft tumors [58]. While the authors highlight the qualitative nature of IVIS imaging, it the results from IVIS show highest organ accumulation in liver and spleen, while from homogenate organ analysis the highest accumulation is measured in liver and tumor, highlighting the potentially misleading results coming from ex vivo comparison across different organs. Van De Ven et al. [11] utilized both confocal imaging and ICP-AES to quantify silicon microparticle biodistribution. While the overall behaviors are similar, with confocal they report lower liver accumulation relative to spleen, which can be explained by a tissue attenuation of fluorescence in optically dense organs such as the liver [50].

Notably, both IVIS and confocal microscopy are limited in evaluating circulating particles (blood). Moreover, the amount of free fluorophore found in kidneys is too low to be detected with either technique, as expected from particle size cutoff for kidneys uptake (5–8 nm) [32].

Even after background subtraction, IVIS imaging underestimated accumulation values in liver, spleen and kidneys, which is a result of intrinsic fluorescence attenuation in densely packed and optically dark organs. This confirms the dramatic effect of organ absorption in optical measurements, which conversely was accounted for in homogenized organs with the use of correction factors. Confocal imaging does not suffer from organ attenuation errors, which is reflected in the improved reconstructed signal in the spleen. However, it is limited in its capability to reconstruct whole organ fluorescence, especially for bigger organs, such as the liver. In these cases, substantially more tissue sections would be needed to obtain a better estimate.

Among all methods, we defined as quantitative those where it was possible to calculate the %ID/g or %ID/organ: ICP-OES, fluorescence of homogenized organs, and radiolabeling. These three quantitative methods all exhibit good accuracy, sensitivity and precision. The results indicate that both fluorescence and radiolabeling are sensitive enough to detect PSPs in blood and kidneys. However, ICP-OES measurements exhibited significantly higher r%, while fluorescence measurements of homogenized organs and radiolabeling yielded similar results. Interestingly, kidney signal in ICP-OES measurements is absent, which is compatible with the size cutoff of kidney uptake (5–8 nm) [32]. However, some signal is detected with fluorescence of homogenized organs, which indicates that some free fluorophore loss is present. The presence of free fluorophore may explain the differences between biodistribution measured from fluorescence of organ homogenates compared to ICP and radiolabeling. In case of radiolabeling, minimal signal is present in the kidneys, which is consistent with minimal labeling loss *in vivo* with radiolabeling. While results from these three methods are comparable, some differences are still evident. This behavior is consistent with previous work, where two ore more technique were used to evaluate biodistribution, resulting in a general agreement of results with some discrepancies. For example, Achraf et al. have measured biodistribution of $^{22}$Na-labeld silica nanoparticles via radioactivity measurement and ICP-MS. Interestingly, their result show a significantly decreased signal in both liver and spleen when measured with gamma counter vs ICP-MS [59]. Liu et al. used IVIS, fluorescence, and radioactivity techniques to investigate the biodistribution of lipid/

calcium/phosphate nanoparticles in tumor-bearing mice [19]. They have found a discrepancy between the three techniques, with radioactive labeling showing dominant accumulation in liver and spleen where fluorescent imaging showed the highest accumulation in tumors.

To overcome limitations of each individual method, while exploiting their advantages, several of these methods should be used in combination when possible. For example, Tanei et al. used ICP to quantitatively characterize particle accumulation in terms of %ID while they used confocal microscopy to quantify the different number of macrophages in the field of view upon different treatments [60]. Similarly, Simon-Gracia et al. used radiolabeling and PET imaging to quantitatively measured biodistribution in whole organs, while confocal microscopy was used to quantify co-localization of polymersomes with macrophages within tumors [61].

In Table 1 all five analyzed methods are compared in terms of general properties. It should be noted that while the procedures and comparison metrics employed here hold general validity, results are protocol, particle, and instrument specific. Thus, the following considerations should be interpreted within the validity range. First, while IVIS and confocal present clear advantages in terms of time requirement (IVIS) and potential for obtaining mechanistic insights through integration with immunofluorescence assays (confocal microscopy), they should both be considered qualitative investigative methods, and always be associated with a quantitative method when quantitative biodistribution results are required. Of the three methods, ICP-OES presents an advantage in terms of it being a direct detection method, even though measurements are not extremely sensitive. Radiolabeling demonstrated to have overall very high sensitivity and precision. In particular, radiolabeling errors on %ID/organ measurements were significantly smaller than values obtained with fluorescence, especially for bigger organs. This effect can be attributed to the fact that radiolabeling allows the direct measurement of the total organ content, without the need of fractioning or dilution. However, it must be noted that radiolabeling protocols may not be always accessible as they require specially trained personnel and dedicated facilities, as well as are constrained by isotope production and decay schedules. Biodistribution measurement of fluorescence in homogenized organs presents an advantage when in complement with other fluorescence-detection methods, since it allows comparison of different results on the same platform, with a single labeling protocol. This can be particularly advantageous with multifunctional platforms developed to be intrinsically fluorescent [51].

While the results discussed here are based on a porous silicon microparticle platform, the validity of the comparison can be extended to other platforms, as the main goal was to evaluate method performances.

## 5 Conclusions

This study presents a systematic comparison of results and performances of different *in vivo* biodistribution methods for injectable porous silicon particles. The major innovation component of this study lies in the use of a single, well characterized particle platform, to evaluate performance of different methods side-by-side. The approach presented here

relies on highly quantitative characterization of sensitivity and precision for each method. These results can be used as a guide to choose and complement the use for biodistribution detection methods for injectable inorganic vectors, based on study purpose and resources. Furthermore, criteria and comparison metrics employed here can be extended to different platforms and methodologies, as they are developed. With proper measures of care, the approach and results presented here can be used to investigate, compare, and optimize biodistribution methods of other vectors such as nanoparticles or molecular drugs.

## Supplementary Material

Refer to Web version on PubMed Central for supplementary material.

## Acknowledgments

M. F. gratefully acknowledges support through NIH/NCI center grant U54CA210181, NIH/NCI NIH/NCI R01CA222959, DoD Breast Cancer Research Breakthrough Level IV Award W81XWH-17-1-0389, and his Ernest Cockrell Jr. Presidential Distinguished Chair at Houston Methodist Research Institute. S.N. acknowledges supports from the Applied Physics Graduate Program, Smalley-Curl Institute at Rice University, Houston, TX.

## References

[1]. Trofimov AD, Ivanova AA, Zyuzin MV, Timin AS, Porous inorganic carriers based on silica, calcium carbonate and calcium phosphate for controlled/modulated drug delivery: fresh outlook and future perspectives, Pharmaceutics 10 (4) (2018).

[2]. Savage DJ, Liu X, Curley SA, Ferrari M, Serda RE, Porous silicon advances in drug delivery and immunotherapy, Curr. Opin. Pharmacol. 13 (5) (2013) 834–841. [PubMed: 23845260]

[3]. Tanaka T, Godin B, Bhavane R, Nieves-Alicea R, Gu J, Liu X, Chiappini C, Fakhoury JR, Amra S, Ewing A, Li Q, Fidler IJ, Ferrari M, In vivo evaluation of safety of nanoporous silicon carriers following single and multiple dose intravenous administrations in mice, Int. J. Pharm. 402 (1–2) (2010) 190–197. [PubMed: 20883755]

[4]. Shahbazi MA, Hamidi M, Makila EM, Zhang H, Almeida PV, Kaasalainen M, Salonen JJ, Hirvonen JT, Santos HA, The mechanisms of surface chemistry effects of mesoporous silicon nanoparticles on immunotoxicity and biocompatibility, Biomaterials 34 (31) (2013) 7776–7789. [PubMed: 23866976]

[5]. Tzur-Balter A, Shatsberg Z, Beckerman M, Segal E, Artzi N, Mechanism of erosion of nanostructured porous silicon drug carriers in neoplastic tissues, Nat. Commun. 6 (2015) 6208. [PubMed: 25670235]

[6]. Wilhelm S, Tavares AJ, Dai Q, Ohta S, Audet J, Dvorak HF, Chan WCW, Analysis of nanoparticle delivery to tumours, Nat. Rev. Mater. 1 (2016) 16014.

[7]. Tsoi KM, MacParland SA, Ma XZ, Spetzler VN, Echeverri J, Ouyang B, Fadel SM, Sykes EA, Goldaracena N, Kaths JM, Conneely JB, Alman BA, Selzner M, Ostrowski MA, Adeyi OA, Zilman A, McGilvray ID, Chan WC, Mechanism of hard-nanomaterial clearance by the liver, Nat. Mater. 15 (11) (2016) 1212–1221. [PubMed: 27525571]

[8]. Dogra P, Adolphi NL, Wang Z, Lin YS, Butler KS, Durfee PN, Croissant JG, Noureddine A, Coker EN, Bearer EL, Cristini V, Brinker CJ, Establishing the effects of mesoporous silica nanoparticle properties on in vivo disposition using imaging-based pharmacokinetics, Nat. Commun. 9 (1) (2018) 4551. [PubMed: 30382084]

[9]. Arms L, Smith DW, Flynn J, Palmer W, Martin A, Woldu A, Hua S, Advantages and limitations of current techniques for analyzing the biodistribution of nanoparticles, Front. Pharmacol. 9 (2018) 802. [PubMed: 30154715]

[10]. Kunjachan S,Ehling J, Storm G, Kiessling F, Lammers T, Noninvasive imaging of nanomedicines and nanotheranostics: principles, progress, and prospects, Chem. Rev. 115 (19) (2015) 10907–10937. [PubMed: 26166537]

[11]. Van de Ven AL, Kim P, Haley O, Fakhoury JR, Adriani G, Schmulen J, Moloney P, Hussain F, Ferrari M, Liu X, Yun SH, Decuzzi P, Rapid tumoritropic accumulation of systemically injected plateloid particles and their biodistribution, J. Control. Release 158 (1) (2012) 148–155. [PubMed: 22062689]

[12]. Godin B, Gu J, Serda RE, Ferrati S, Liu X, Chiappini C, Tanaka T, Decuzzi P, Ferrari M, Multistage mesoporous silicon-based nanocarriers: biocompatibility with immune cells and controlled degradation in physiological fluids, Controll. Release Newsl. 25 (4) (2008) 9–11. [PubMed: 21853161]

[13]. Godin B, Chiappini C, Srinivasan S, Alexander JF, Yokoi K, Ferrari M, Decuzzi P, Liu X, Discoidal porous silicon particles: fabrication and biodistribution in breast cancer bearing mice, Adv. Funct. Mater. 22 (20) (2012) 4225–4235. [PubMed: 23227000]

[14]. Chinde S, Grover P, Toxicological assessment of nano and micron-sized tungsten oxide after 28 days repeated oral administration to Wistar rats, Mutat. Res. 819 (2017) 1–13.

[15]. Al Zaki A, Hui JZ, Higbee E, Tsourkas A, Biodistribution, clearance, and toxicology of polymeric micelles loaded with 0.9 or 5 nm gold nanoparticles, J. Biomed. Nanotechnol 11 (10) (2015) 1836–1846. [PubMed: 26502646]

[16]. Tanaka T, Mangala LS, Vivas-Mejia PE, Nieves-Alicea R, Mann AP, Mora E, Han HD, Shahzad MM, Liu X, Bhavane R, Gu J, Fakhoury JR, Chiappini C, Lu C, Matsuo K, Godin B, Stone RL, Nick AM, Lopez-Berestein G, Sood AK, Ferrari M, Sustained small interfering RNA delivery by mesoporous silicon particles, Cancer Res. 70 (9) (2010) 3687–3696. [PubMed: 20430760]

[17]. Ganesh S, Iyer AK, Gattacceca F, Morrissey DV, Amiji MM, In vivo biodistribution of siRNA and cisplatin administered using CD44-targeted hyaluronic acid nanoparticles, J. Control. Release 172 (3) (2013) 699–706. [PubMed: 24161254]

[18]. Coll JL, Cancer optical imagingusing fluorescent nanoparticles, Nanomedicine (Lond.) 6 (1) (2011) 7–10. [PubMed: 21182412]

[19]. Liu Y, Tseng YC, Huang L, Biodistribution studies of nanoparticles using fluorescence imaging: a qualitative or quantitative method?, Pharm Res. 29 (12) (2012) 3273–3277. [PubMed: 22806405]

[20]. Vats M, Mishra SK, Baghini MS, Chauhan DS, Srivastava R, De A, Near infrared fluorescence imaging in nano-therapeutics and photo-thermal evaluation, Int. J. Mol. Sci. (2017) 18(5).

[21]. Lee MJ, Veiseh O, Bhattarai N, Sun C, Hansen SJ, Ditzler S, Knoblaugh S, Lee D, Ellenbogen R, Zhang M, Olson JM, Rapid pharmacokinetic and biodistribution studies using cholorotoxin-conjugated iron oxide nanoparticles: a novel non-radioactive method, PLoS ONE 5 (3) (2010) e9536. [PubMed: 20209054]

[22]. Cong Z, Yang F, Cao L, Wen H, Fu T, Ma S, Liu C, Quan L, Liao Y, Multispectral optoacoustic tomography (MSOT) for imaging the particle size- dependent intratumoral distribution of polymeric micelles, Int. J Nanomed. 13 (2018) 8549–8560.

[23]. Gusliakova O, Atochina-Vasserman EN, Sindeeva O, Sindeev S, Pinyaev S, Pyataev N, Revin V, Sukhorukov GB, Gorin D, Gow AJ, Use of submicron vaterite particles serves as an effective delivery vehicle to the respiratory portion of the lung, Front. Pharmacol. 9 (2018) 559. [PubMed: 29915536]

[24]. Kumar V, Mundra V, Peng Y, Wang Y, Tan C, Mahato RI, Pharmacokinetics and biodistribution of polymeric micelles containing miRNA and small- molecule drug in orthotopic pancreatic tumor-bearing mice, Theranostics 8 (15)(2018) 4033–4049. [PubMed: 30128034]

[25]. Hollis CP, Weiss HL, Leggas M, Evers BM, Gemeinhart RA, Li T, Biodistribution and bioimaging studies of hybrid paclitaxel nanocrystals: lessons learned of the EPR effect and image-guided drug delivery, J. Control. Release 172 (1) (2013) 12–21. [PubMed: 23920039]

[26]. Vasconcelos DM, Ribeiro-da-Silva M, Mateus A, Alves CJ, Machado GC, Machado-Santos J, Paramos-de-Carvalho D, Alencastre IS, Henrique R, Costa G, Barbosa MA, Lamghari M, Immune response and innervation signatures in aseptic hip implant loosening, J. Transl. Med. 14 (1) (2016) 205. [PubMed: 27387445]

[27]. Bernhard W, El-Sayed A, Barreto K, Gonzalez C, Hill W, Parada AC, Fonge H, Geyer CR, Near infrared fluorescence imaging of EGFR expression in vivo using IRDye800CW-nimotuzumab, Oncotarget 9 (5) (2018) 6213–6227. [PubMed: 29464066]

[28]. Oliveira S, Cohen R, Walsum MS, van Dongen GA, Elias SG, van Diest PJ, Mali W, van PM Bergen En Henegouwen, A novel method to quantify IRDye800CW fluorescent antibody probes ex vivo in tissue distribution studies, EJNMMI Res. 2 (1) (2012) 50. [PubMed: 23009555]

[29]. Wolfram J, Nizzero S, Liu H, Li F, Zhang G, Li Z, Shen H, Blanco E, Ferrari M, A chloroquine-induced macrophage-preconditioning strategy for improved nanodelivery, Sci. Rep. 7 (1) (2017) 13738. [PubMed: 29062065]

[30]. Chiappini C, Tasciotti E, Fakhoury JR, Fine D, Pullan L, Wang YC, Fu L, Liu X, Ferrari M, Tailored porous silicon microparticles: fabrication and properties, ChemPhysChem 11 (5) (2010) 1029–1035. [PubMed: 20162656]

[31]. Tasciotti E, Liu X, Bhavane R, Plant K, Leonard AD, Price BK, Cheng MM, Decuzzi P, Tour JM, Robertson F, Ferrari M, Mesoporous silicon particles as a multistage delivery system for imaging and therapeutic applications, Nat. Nanotechnol. 3 (3) (2008) 151–157. [PubMed: 18654487]

[32]. Longmire M, Choyke PL, Kobayashi H, Clearance properties of nano-sized particles and molecules as imaging agents: considerations and caveats, Nanomedicine (Lond.) 3 (5) (2008) 703–717. [PubMed: 18817471]

[33]. Blanco E, Shen H, Ferrari M, Principles of nanoparticle design for overcoming biological barriers to drug delivery, Nat. Biotechnol. 33 (9) (2015) 941–951. [PubMed: 26348965]

[34]. Venuta A, Wolfram J, Shen H, Ferrari M, Post-nano strategies for drug delivery: multistage porous silicon microvectors, J. Mater. Chem. B 5 (2) (2017) 207–219. [PubMed: 28670454]

[35]. Godin B, Tasciotti E, Liu X, Serda RE, Ferrari M, Multistage nanovectors: from concept to novel imaging contrast agents and therapeutics, Acc. Chem. Res. 44 (10) (2011) 979–989. [PubMed: 21902173]

[36]. Godin B, Gu J, Serda RE, Bhavane R, Tasciotti E, Chiappini C, Liu X, Tanaka T, Decuzzi P, Ferrari M, Tailoring the degradation kinetics of mesoporous silicon structures through PEGylation, J. Biomed. Mater. Res. A 94 (4) (2010) 1236–1243. [PubMed: 20694990]

[37]. Xu R, Zhang G, Mai J, Deng X, Segura-Ibarra V, Wu S, Shen J, Liu H, Hu Z, Chen L, Huang Y, Koay E, Huang Y, Liu J, Ensor JE, Blanco E, Liu X, Ferrari M, Shen H, An injectable nanoparticle generator enhances delivery of cancer therapeutics, Nat. Biotechnol. 34 (4) (2016) 414–418. [PubMed: 26974511]

[38]. Shen J, Wu X, Lee Y, Wolfram J, Yang Z, Mao ZW, Ferrari M, Shen H, Porous silicon microparticles for delivery of siRNA therapeutics, J. Vis. Exp. 95 (2015) 52075.

[39]. Zhang J, Mai J, Li F, Shen J, Zhang G, Li J, Hinkle LE, Lin D, Liu X, Li Z, Wang RF, Mittendorf EA, Ferrari M, Shen H, Investigation of parameters that determine Nano-DC vaccine transport, Biomed. Microdevices 21 (2) (2019) 39. [PubMed: 30949852]

[40]. Wolfram J, Shen H, Ferrari M, Multistage vector (MSV) therapeutics, J. Control. Release 219 (2015) 406–415. [PubMed: 26264836]

[41]. Shen H, You J, Zhang G, Ziemys A, Li Q, Bai L, Deng X, Erm DR, Liu X, Li C, Ferrari M, Cooperative, nanoparticle-enabled thermal therapy of breast cancer, Adv. Healthc. Mater. 1 (1) (2012) 84–89. [PubMed: 23184690]

[42]. Shen H, Rodriguez-Aguayo C, Xu R, Gonzalez-Villasana V, Mai J, Huang Y, Zhang G, Guo X, Bai L, Qin G, Deng X, Li Q, Erm DR, Aslan B, Liu X, Sakamoto J, Chavez-Reyes A, Han HD, Sood AK, Ferrari M, Lopez-Berestein G, Enhancing chemotherapy response with sustained EphA2 silencing using multistage vector delivery, Clin. Cancer Res. 19 (7) (2013) 1806–1815. [PubMed: 23386691]

[43]. Martinez JO, Evangelopoulos M, Chiappini C, Liu X, Ferrari M, Tasciotti E, Degradation and biocompatibility of multistage nanovectors in physiological systems, J. Biomed. Mater. Res. A 102 (10) (2014) 3540–3549. [PubMed: 25269799]

[44]. Shen J, Xu R, Mai J, Kim HC, Guo X, Qin G, Yang Y, Wolfram J, Mu C, Xia X, Gu J, Liu X, Mao ZW, Ferrari M, Shen H, High capacity nanoporous silicon carrier for systemic delivery of gene silencing therapeutics, ACS Nano 7 (11) (2013)9867–9880. [PubMed: 24131405]

[45]. Mai J, Huang Y, Mu C, Zhang G, Xu R, Guo X, Xia X, Volk DE, Lokesh GL, Thiviyanathan V, Gorenstein DG, Liu X, Ferrari M, Shen H, Bone marrow endothelium-targeted therapeutics for metastatic breast cancer, J. Control. Release 187 (2014) 22–29. [PubMed: 24818768]

[46]. Nizzero S, Ziemys A, Ferrari M, Transport barriers and oncophysics in cancer treatment, Trends Cancer 4 (4) (2018) 277–280. [PubMed: 29606312]

[47]. Godin B, Chiappini C, Srinivasan S, Alexander JF, Yokoi K, Ferrari M, Decuzzi P, Liu X, Discoidal porous silicon particles: fabrication and biodistribution in breast cancer bearing mice, Adv. Funct. Mater. (2012).

[48]. Evangelopoulos M, Parodi A, Martinez JO, Yazdi IK, Cevenini A, van de Ven AL, Quattrocchi N, Boada C, Taghipour N, Corbo C, Brown BS, Scaria S, Liu X, Ferrari M, Tasciotti E, Cell source determines the immunological impact of biomimetic nanoparticles, Biomaterials 82 (2016) 168–177. [PubMed: 26761780]

[49]. Gatto Monticone D, Katamadze K, Traina P, Moreva E, Forneris J, Ruo- Berchera I, Olivero P, Degiovanni IP, Brida G, Genovese M, Beating the Abbe diffraction limit in confocal microscopy via nonclassical photon statistics, Phys. Rev. Lett. 113 (14) (2014) 143602. [PubMed: 25325642]

[50]. Colin M, Moritz S, Schneider H, Capeau J, Coutelle C, Brahimi-Horn MC, Haemoglobin interferes with the ex vivo luciferase luminescence assay: consequence for detection of luciferase reporter gene expression in vivo, Gene Ther. 7 (15) (2000) 1333–1336. [PubMed: 10918505]

[51]. Mattu C, Brachi G, Menichetti L, Flori A, Armanetti P, Ranzato E, Martinotti S, Nizzero S, Ferrari M, Ciardelli G, Alternating block copolymer- based nanoparticles as tools to modulate the loading of multiple chemotherapeutics and imaging probes, Acta Biomater. (2018).

[52]. Ricco R, Nizzero S, Penna E, Meneghello A, Cretaio E, Enrichi F, Ultra-small dye-doped silica nanoparticles via modified sol-gel technique, J. Nanopart. Res. 20 (5) (2018) 117. [PubMed: 29720891]

[53]. Koo V, Hamilton PW, Williamson K, Non-invasive in vivo imaging in small animal research, Cell Oncol. 28 (4) (2006) 127–139. [PubMed: 16988468]

[54]. Robson AL, Dastoor PC, Flynn J, Palmer W, Martin A, Smith DW, Woldu A, Hua S, Advantages and limitations of current imaging techniques for characterizing liposome morphology, Front. Pharmacol. 9 (2018) 80. [PubMed: 29467660]

[55]. Pillay CS, Elliott E, Dennison C, Endolysosomal proteolysis and its regulation, Biochem. J. 363 (Pt 3) (2002) 417–429. [PubMed: 11964142]

[56]. Chen AK, Cheng Z, Behlke MA, Tsourkas A, Assessing the sensitivity of commercially available fluorophores to the intracellular environment, Anal. Chem. 80 (19) (2008) 7437–7444. [PubMed: 18700780]

[57]. Graber ML, DiLillo DC, Friedman BL, Pastoriza-Munoz E, Characteristics of fluoroprobes for measuring intracellular pH, Anal. Biochem. 156 (1) (1986) 202–212. [PubMed: 3740410]

[58]. Diagaradjane P, Orenstein-Cardona JM, Colon-Casasnovas NE, Deorukhkar A, Shentu S, Kuno N, Schwartz DL, Gelovani JG, Krishnan S, Imaging epidermal growth factor receptor expression in vivo: pharmacokinetic and biodistribution characterization of a bioconjugated quantum dot nanoprobe, Clin. Cancer Res. 14 (3) (2008) 731–741. [PubMed: 18245533]

[59]. Al Faraj A, Alotaibi B, Shaik AP, Shamma KZ, Al Jammaz I, Gerl J, Sodium- 22-radiolabeled silica nanoparticles as new radiotracer for biomedical applications: in vivo positron emission tomography imaging, biodistribution, and biocompatibility, Int. J. Nanomed. 10 (2015) 6293–6302.

[60]. Tanei T, Leonard F, Liu X, Alexander JF, Saito Y, Ferrari M, Godin B, Yokoi K, Redirecting transport of nanoparticle albumin-bound paclitaxel to macrophages enhances therapeutic efficacy against liver metastases, Cancer Res. 76 (2) (2016) 429–439. [PubMed: 26744528]

[61]. Simon-Gracia L, Scodeller P, Fuentes SS, Vallejo VG, Rios X, San Sebastian E, Sidorenko V, Di Silvio D, Suck M, De Lorenzi F, Rizzo LY, von Stillfried S, Kilk K, Lammers T, Moya SE, Teesalu T, Application of polymersomes engineered to target p32 protein for detection of small breast tumors in mice, Oncotarget 9 (27) (2018) 18682–18697. [PubMed: 29721153]

## Statement of Significance

The significance of this work lies in the use of a single platform to test performances of different biodistribution methods *in vivo*, with a strict quantitative metric. These results, united with the qualitative comparison of advantages and disadvantages of each technique, are aimed at supporting the rational choice of each different method according to the specific application, to improve the quantitative description of biodistribution results that will be published by others in the future.

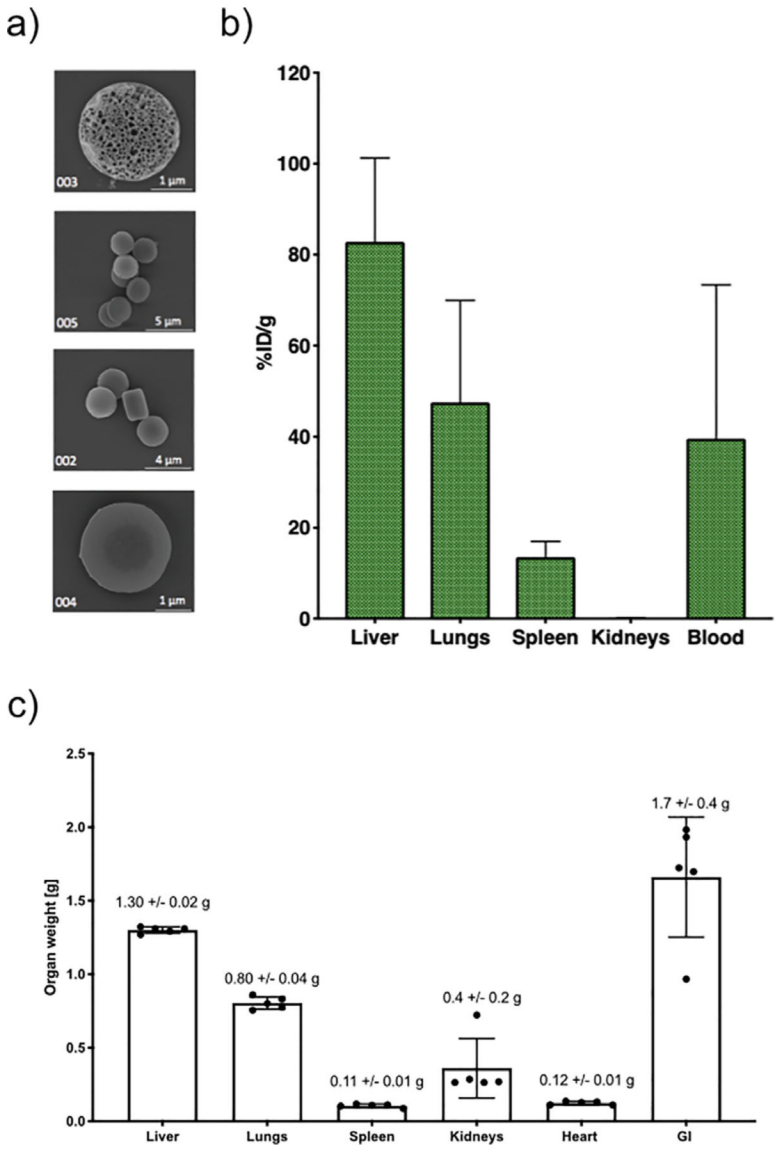


**Fig. 1.**

Particle biodistribution estimated through inductively coupled plasma- optical emission spectroscopy (ICP-OES). a) Scanning electron microscopy (SEM) of discoidal PSPs. b) PSP biodistribution as measured through ICP-OES presented as % ID/g. c) Average organ weights in g.

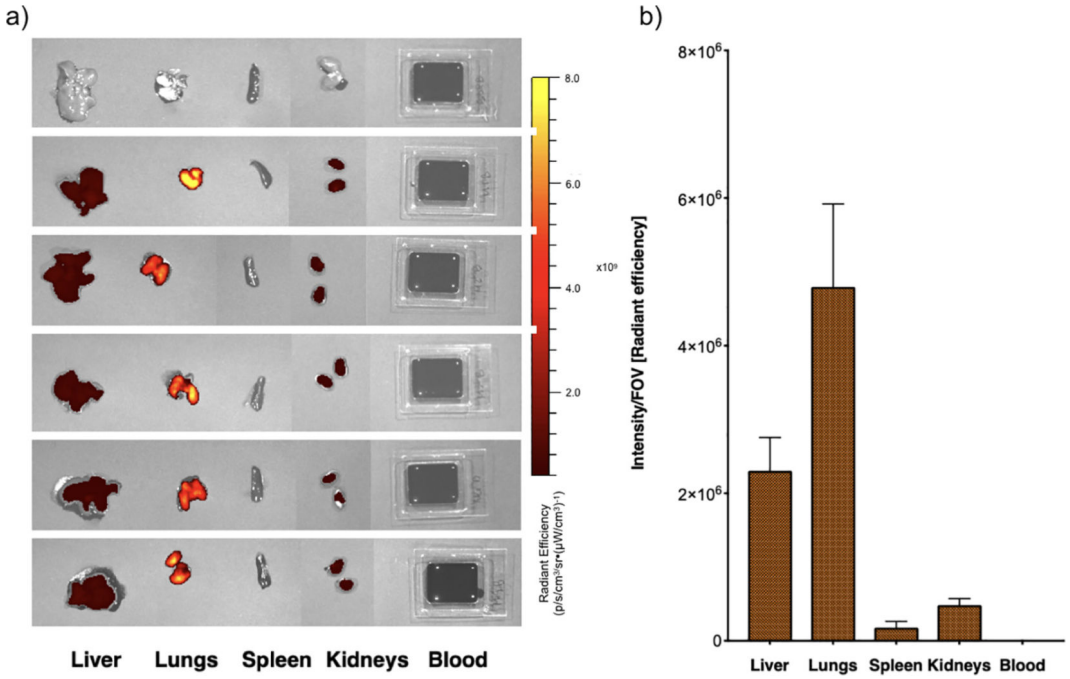


**Fig. 2.**

Particle biodistribution with IVIS. a) Radiant efficiency of individual organs 15min after injection of Alexa 647-labeled PSPs (Ex = 640nm, Em = 680nm, exposure = 0.5 s). b) PSP biodistribution in single organs measured as intensity/field of view (FOV) (Fig. S1). Results from N = 5 mice are presented as average per organ; error bars represent calculated standard deviation.

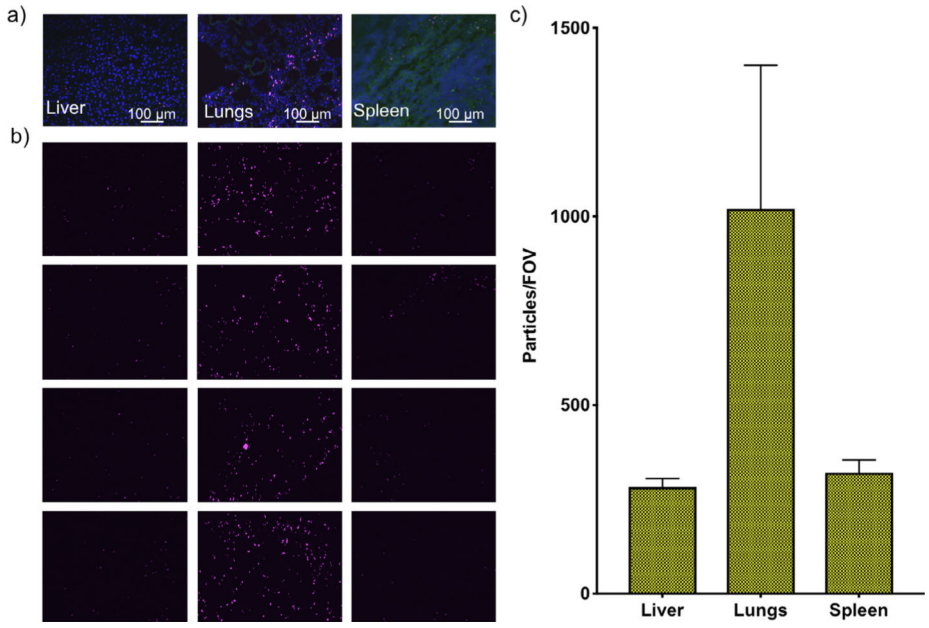


**Fig. 3.**

Particle biodistribution with confocal imaging. a) Representative confocal images of liver, lungs, and spleen acquired with Cy5 filter of Alexa-647-labeled PSPs (DAPI in blue, tissue in green, PSPs in pink). b) Four representative images of the Cy5 channel are reported to show qualitative particle accumulation in different organs. Green channel shows tissue localization. c) PSP biodistribution in single organs measured as intensity over FOV. Between 8 and 15 images obtained with a 20× air objective were analyzed for each organ. Biodistribution estimated with MATLAB algorithm (Fig. S1) analysis of confocal images. Results are presented as average per slide; error bars represent calculated standard deviation. (For interpretation of the references to colour in this figure legend, the reader is referred to the web version of this article.)

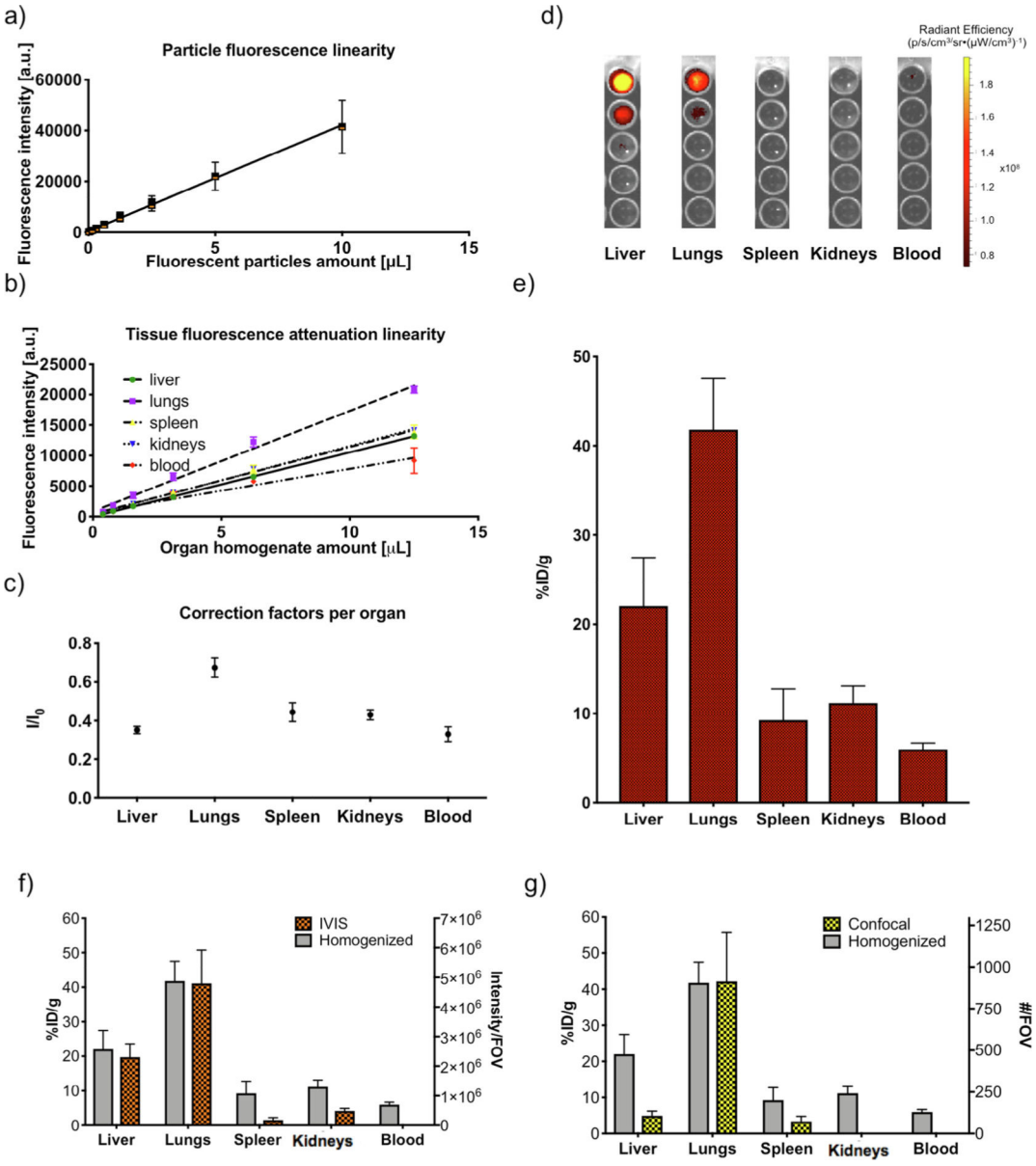


**Fig. 4.**

Particle biodistribution with fluorescence measurement of homogenized organs. a) Measurements of fluorescence emission linearity within the Alexa-647-labeled PSPs dilution range of the biodistribution experiment ($R^2$ = 0.94). The x-axis shows the particle volume dispersed in 100 µL of PBS, from a solution containing 320 million PSPs/mL. b) Measurements of linearity of tissue attenuation by addition of Alexa-647-labeled PSPs to homogenized tissue ($R^2$ = 0.99 for liver, lungs, spleen, kidneys, $R^2$ = 0.93 or blood). c) Measurements of the tissue attenuation coefficient calculated as the average of the ratios between fluorescence of PSPs in phosphate buffered saline (PBS) (true fluorescence, I) divided by the fluorescence of the same amount of PSPs dispersed in organ homogenate (attenuated fluorescence $I_0$). d) Serial dilutions images of homogenized organs used for plate reader measurements. Intensities are measured for all dilutions with a plate reader (ex =

640 nm, em = 678 nm, slit aperture 20/20). e) %ID/g calculated from fluorescence emission from the tissue well with the use of the correction factor. f) Visual comparison of results from IVIS and fluorescence from homogenized organs. g) Visual comparison of results from confocal imaging and fluorescence from homogenized organs.

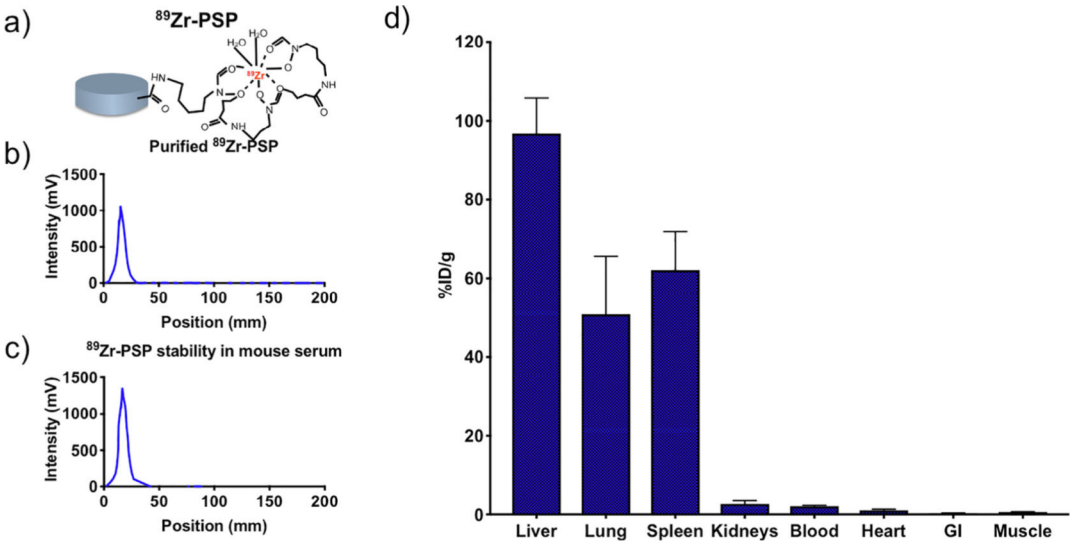


**Fig. 5.**

Particle biodistribution estimated through radiolabeling. a) Schematic of DFO chelation and 89Zr labeling. b) Radioactivity intensity peak for labeled PSP in PBS, immediately after synthesis and purification. c) Radioactivity intensity peak for labeled PSP, 1 h after incubation in mouse plasma (1:1 vol dilution in PBS). d) Biodistribution as measured via radioactivity detection of radiolabeled particles.

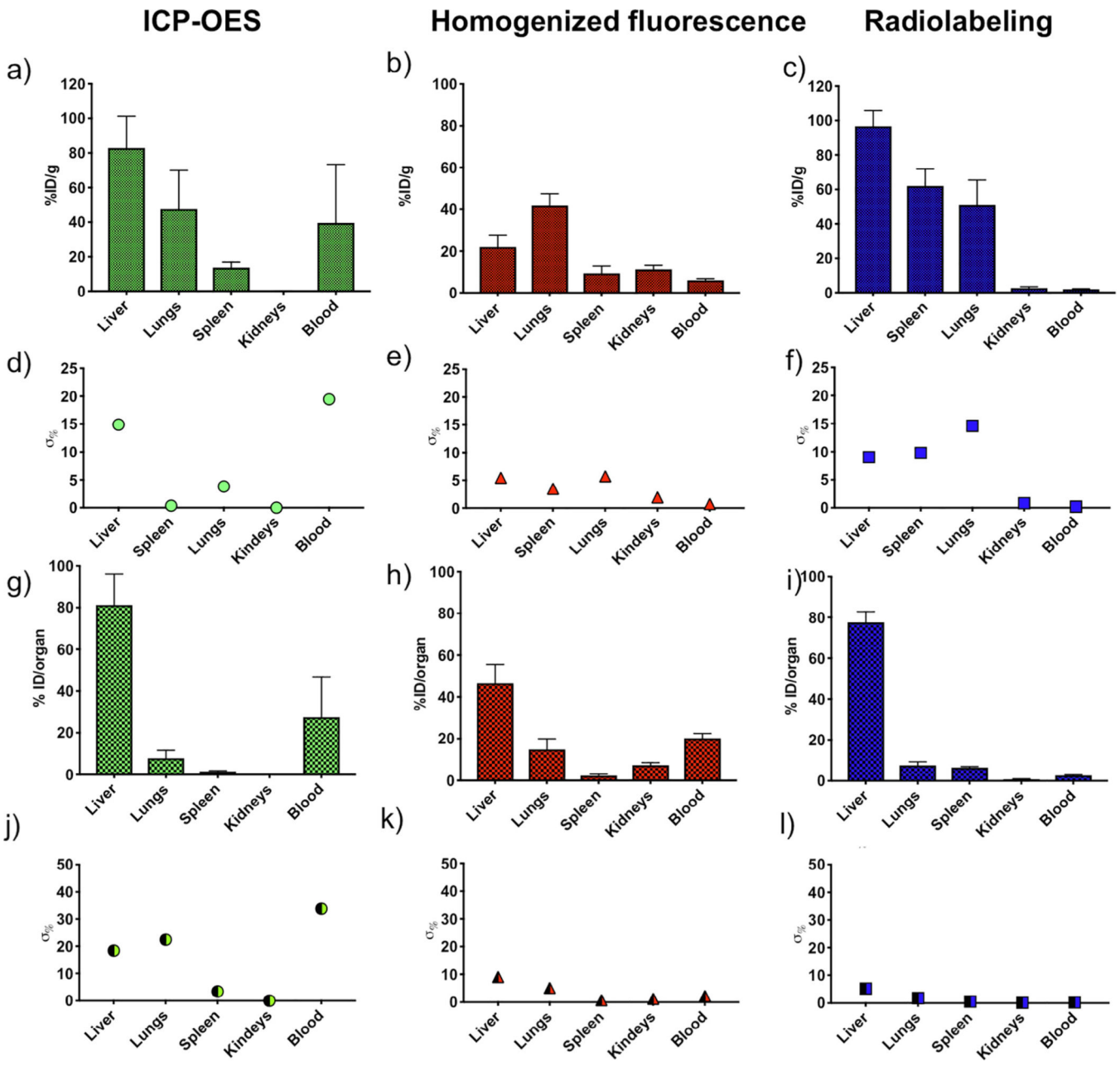


**Fig. 6.**

Comparison of biodistribution methods. Biodistribution is reported as %ID/g when such calculation is possible: a) ICP-OES, b) fluorescence of homogenized organs, and c) radiolabeling, with calculated percentage errors of d) ICP-OES, e) fluorescence, and f) radiolabeling. Biodistribution is reported as %ID/organ when such calculation is possible: g) ICP-OES, h) fluorescence of homogenized organs, and i) radiolabeling, with calculated percentage errors of j) ICP-OES, k) fluorescence, and l) radiolabeling. Results from N = 5 mice are presented as average per organ; error bars represent calculated standard deviation.

**Table 1**

Comparison across methods. Five biodistribution methods have been systematically compared and evaluated side by side.

| Method | Labeling | Representativity | Advantages | Disadvantages |
|---|---|---|---|---|
| ICP-OES | None | Whole organ (through estimate) | • Direct detection method | • Time consuming<br>• Only inorganic particles |
| IVIS | Fluorescent | Surface | • Time efficient<br>• Immediate result | • No deep tissue properties<br>• Only same-organ comparison |
| Confocal | Fluorescent | Section | • High spacial resolution<br>• Potential for mechanistic understanding<br>• Resolves local heterogeneity | • No whole organ properties<br>• Biased on local heterogeneity |
| Homogenized fluorescence | Fluorescent | Whole organ (through estimate) | • Highly accessible (protocols and instrumentation)<br>• Offers integration with other fluorescent assays<br>• Intrinsically fluorescent platforms | • Time consuming |
| Radiolabeling | Radioactive | Whole organ (through direct measurement) | • Extremely sensitive method<br>• Time efficient<br>• Direct measurement of whole organ properties | • Requires specially trained personnel and dedicated facilities<br>• Constraining scheduling (production and decay) |